Functionalization of Monolithic MOF Thin Films with Hydrocarbon Chains to Achieve Superhydrophobic Surfaces with Tunable Water Adhesion Strength

Evgenia Bogdanova,[1,+] Modan Liu,[1,+] Patrick Hodapp,[2] Angana Borbora[5] Wolfgang Wenzel,[6] Stefan Bräse,[3],[4] André Jung,[3] Zheqin Dong,[3] Pavel Levkin,[3,4] Uttam Manna,* [5],[7] Tawheed Hashem,* [1] and Christof Wöll*[1]

[1] Karlsruhe Institute of Technology (KIT), Institute of Functional Interfaces (IFG), Hermann-von-Helmholtz Platz-1, 76344 Eggenstein-Leopoldshafen (Germany)

[2] Karlsruhe Institute of Technology (KIT), Institute for Biological Interfaces – Soft Matter Synthesis Laboratory (IBG3 – SML), Kaiserstrasse 12, 76131 Karlsruhe (Germany)

[3] Karlsruhe Institute of Technology (KIT), Institute of Biological and Chemical Systems (IBCS-FMS), Kaiserstrasse 12, 76131 Karlsruhe (Germany)

[4] Karlsruhe Institute of Technology (KIT), Institute of Organic Chemistry (IOC), Kaiserstrasse 12, 76131 Karlsruhe (Germany)

[5] Indian Institute of Technology Guwahati (IITG), Department of Chemistry, Assam, 781039 India

[6] Karlsruhe Institute of Technology (KIT), Institute of Nanotechnology (INT), Hermann-von-Helmholtz Platz-1, 76344 Eggenstein-Leopoldshafen (Germany)

[7] Indian Institute of Technology Guwahati (IITG), Centre for Nanotechnology, Assam 781039 India

Correspondence to: Christof Wöll, email: christof.woell@kit.edu

Supporting Information. This section offers experimental details on the layer-by-layer fabrication of SURMOFs along with XRD data which are used to derive MOF structural information. Additionally, results from mass spectroscopy (LC-MS) and from atomic force microscopy (AFM) are presented. Detailed discussions on the difference in flexibility of the SAM and the hydrocarbons grafted to the SURMOF and the entropic states are summarized based on the Ramachandran plots of the separate systems of SAM@Au, C18F@SURMOF, and C18@SURMOF.

Materials

Chemicals used for synthesizing UiO-66-NH_2 SURMOF

The following reagents were purchased from Germany and Saudi Arabia to prepare UiO-66 NH_2 SURMOF: zirconium (IV) chloride ($ZrCl_4$, reactor grade, 99.5%) and 2-aminoterephthalic acid (99%, NH_2-BDC) were used as metal ions and organic linker sources, respectively. N,N-Dimethylformamide (DMF) was supplied by Emsure Company and was used as a solvent for both metal ions and linker compound, as well as an intermediate washer for prepared samples. All reagents were used without further purification.

Chemicals used for SURMOF modification

Triethylamine (TEA, 99.0%) was obtained from Merck, USA, octadecanoyl chloride (97%) was provided by Sigma-Aldrich, USA, and tetrahydrofuran (THF, 99%) was supplied by VWR, EC. Moreover, perfluorooctadecanoic acid (95%) was provided by abcr, Germany, whereas both pyridine (99.5%, United Kingdom) and thionyl dichloride (+99.5%, BE) were supplied by Acros Organics.

Methods

Surface Functionalization

Self-assembled monolayers (SAMs) of 11-mercapto-1-undecanol (MUD, Sigma Aldrich) were employed to functionalize Au-coated silicon wafers. The substrates were left in the dark at room temperature for 48 h with the gold side up in a 1 mM ethanolic solution of MUD, producing an -

OH functionalized surface. To prepare the substrates for immediate use in the synthesis, they were completely washed with pure ethanol and dried in a flow of dry nitrogen.

Synthesis of UiO-66-NH_2 SURMOF

UiO-66-NH_2 was prepared using the following previously reported procedure.[1] Typically, an automated dip coating method using a silar coating system (Holmarc, HO-TH-03B1, India) was utilized to prepare LPE SURMOF of UiO-66-NH_2 on a functionalized gold coated substrate (FGCS). Two different solutions were prepared. Solution A, the metal ion source, is composed of 90 mM of $ZrCl_4$ in 100 mL DMF + 20 mL HCl. Solution B, the organic linker source, is composed of 150 mM of NH_2-BDC dissolved in 100 mL DMF. Both solutions were heated to 80 ℃ and maintained at this temperature during all preparation steps. FGCS was immersed in solution A with stirring at 500 rpm for 90 min and then washed with DMF. Following washing, FGCS was immersed in solution B for 120 min under stirring and then washed with DMF. The process of FGCS immersion in solutions A and B with washing was repeated 30 times to create 30 layers of UiO-66-NH_2 on FGCS. To guarantee complete exchange of guest molecules, the resulting UiO-66-NH_2@FGCS was washed with ethanol six times, followed by immersion in ethanol for 24 h. After the washing process, the samples were left to dry overnight in air.

Surface Roughness Reduction Protocol

The surface roughness of the prepared SURMOF samples was addressed through a treatment process as follows: initially, the prepared SURMOF samples were immersed in dimethylformamide (DMF) for one hour at 90 degrees Celsius. Subsequently, the samples were immersed in ethanol and subjected to sonication for a duration of four hours. Throughout this

period, the ethanol was refreshed every hour. This treatment protocol effectively contributed to the reduction of surface roughness in the UiO-66-NH_2 SURMOF samples.

Syntheses of UiO-66-NH-C18 SURMOF

To synthesize UiO-66-NH-C18 (C18@SURMOF), we immersed the synthesized UiO-66-NH_2 SURMOF in a glass container having triethylamine solution diluted with DMF. The glass container was then placed in an ice bath and gently shaken for one hour, followed by adding a mixture of THF and octadecanoyl chloride (v/v, 1:1). Following that, the produced suspension was heated to 45 ℃ for 24 h. C18@SURMOF was collected after cooling down and washed five times with DMF and methanol.

Syntheses of UiO-66-NH-CF SURMOF

To prepare UiO-66-NH-C18F (C18F@SURMOF), we followed the same procedure as C18@SURMOF, except that we used perfluorooctadecanoyl chloride (provided from perfluorooctadecanoic acid as shown in the supporting information file) instead of octadecanoyl chloride.

Characterization

To investigate the morphology of SURMOFs before and after modification, SEM measurements were conducted using a Field Emission Gun (FEI) Philips XL SERIES 30 ESEM-FEG (FEI Co., Eindhoven, NL). To preclude charging and increase sample's conductivity, all samples were coated with a ~5 nm thick gold/palladium film before recording SEM micrographs. Moreover, all specimens underwent high-vacuum (1.5 Torr) using 20 keV acceleration voltage.

The patterns of powder X-ray diffraction (PXRD) were recorded using an X-ray diffractometer Bruker D8-Advance "DaVinci" in Bragg-Brentano θ-θ geometry and a 192-stripe Lynxeye detector over an angular range of 2θ from 1.5° to 68° with 0.015° 2θ step width and 384 seconds per step, and for porous supports over an angular range of 2θ from 4° to 20° with 0.02° 2θ step width and 83 seconds per step.

Infrared reflection absorption spectroscopy (IRRAS) data was achieved utilizing a Bruker VERTEX 80 purged with dried air. IRRAS accessory (A518) exhibits a fixed angle of incidence of 80°. The data were collected using a narrow-band liquid-nitrogen-cooled mercury cadmium telluride detector. Per-deuterated hexadecanethiol SAMs on Au/Ti/Si were utilized for reference measurements. The data were provided by Amerpcan Nicolet AVATAR 360 FT-IR spectrometers.

The static water contact angle (WCA) was measured using a Dataphysics contact angle meter with a droplet of distilled water (5 μL) at ambient temperature.

Molecular Dynamics Simulations

All-atom molecular dynamics (MD) simulations were conducted to determine the structure of C18 chains grafted to the outer surface of the surface SURMOF, as well as for the investigation of wetting behavior of pristine and modified substrates. To validate this theoretical approach, the wetting behavior of thiolate-based SAMs on Au substrates was simulated using OPLS-AA force field parameters for C18 chains and previously reported protocols[2]. In the case of SURMOF, UFF4MOF force field was adopted for describing the flexible UiO-66-NH_2 SURMOF.[3] C18 chains were modeled via OPLS-AA force field,[4, 5] with parametrization revised from

LigParGen.[6] For all different substrates, water molecules in the wetting simulation were parametrized according to SPC/E model.[7]

LAMMPS package[8] was used to perform MD simulations for grafting and wetting processes. In the grafting simulations, the timestep was set to $\tau = 0.01$ fs in the canonical ensemble under Nose-Hoover thermostat[9] at T = 300K, whereas during the wetting, the simulation timestep was set to $\tau = 0.25$ fs, under Nose-Hoover thermostat[9] and Nose-Hoover-Andersen barostat[10] to model NPT conditions, at ambient pressure p = 1 atm and temperature T = 300 K.

The initial molecular configuration consisted of a 4x4x2 supercell of UiO-66-NH_2 SURMOF. During the simulated grafting, C18 chains were tilted by 5° and artificially placed in the MOF, with the hydrophilic head of the chain within 0.3 nm distance of nitrogen on the -NH_2 on MOF linker. One hydrogen atom on the head section of C18 chain, as well as one hydrogen on -NH_2 group in SURMOF linker, were removed to allow phenomenological bond formation events to occur as a stochastic process. When the carbon from C18 chain is within 0.4 nm of the nitrogen atom in -NH_2 group, with 80% probability, a C–N bond was added to link the hydrocarbon chain and SURMOF, removing the extra hydrogen atoms. The chains which failed to anchor to SURMOF were removed. For the successfully grafted chains, the partial charges on -NH- group and the head of C18 chain were re-assigned by Hartree-Fock method via MOPAC.[11] For the simulation of wetting on a pristine UiO-66-NH_2 MOF, a water "cube" consisting of 1074 water molecules was placed on the top of SURMOF, while for the grafted C18@SURMOF, a water "ball" consisting of 3604 water molecules is placed on the top of grafted chains. The water droplet on SURMOF system was relaxed for 3 ns in MD simulation. After this time, the water contact angle was determined from the geometrical profile of water droplets in MD snapshots using a previously established method.[12]

Synthesis of perfluorooctadecanoyl chloride

In addition to a mixture of perfluorooctadecanoic acid (501 mg) and thionyl dichloride (5 mL), a catalytic amount of pyridine (5 μL) was charged to the flask under stirring. After being equipped with a reflux condenser, the reaction mixture was maintained in an oil bath at 80 °C and stirred for three days. After a 1-day reaction, the mixture was supplemented with extra volume of thionyl dichloride (5 mL).

After cooling down at ambient room temperature, volatiles were removed with rotavap under reduced pressure (180 mbar and 40 °C water bath). The flask with white/yellow powder (perfluorooctadecanoyl chloride) was filled with argon and stored until subsequent utilization.

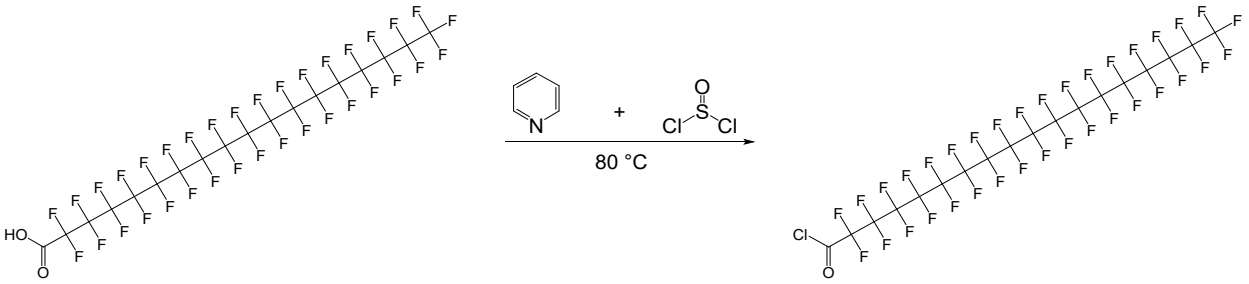

Fig. S1. Schematic illustration of perfluorooctadecanoyl chloride preparation.

Synthesis of

2,2,3,3,4,4,5,5,6,6,7,7,8,8,9,9,10,10,11,11,12,12,13,13,14,14,15,15,16,16,17,17,18,18,18-pentatriacontafluorooctadecanoyl chloride

2,2,3,3,4,4,5,5,6,6,7,7,8,8,9,9,10,10,11,11,12,12,13,13,14,14,15,15,16,16,17,17,18,18,18-pentatriacontafluorooctadecanoic acid (500 mg, 547 μmol, 1.00 equiv) was used as starting

material and refluxed in 5 mL of thionyl chloride (8.20 g, 5.00 mL, 68.9 mmol, 126 equiv) in the presence of catalytic amounts of pyridine (4.90 mg, 5.00 µL, 61.6 µmol, 0.113 equiv) for 90 h. After cooling to 21°C, the volatiles were removed under reduced pressure to yield the acid chloride.

Time-of-Flight Secondary Ion Mass Spectrometry (ToF-SIMS) results

ToF-SIMS was employed to study the surface modification of UiO-66-NH_2 SURMOF. **Fig. S2** displays one blank sample (in black) referring to the pristine SURMOFs before modification and two surface-modified SURMOF samples (in blue and red). Notably, both modified samples are the same to ensure the repeatability of the test results.

The results revealed that Zr^{4+} and Cl^- were easily detected in the blank sample of pristine UiO-66-NH_2 SURMOF (**Fig. S2a, b**). However, upon post-treatment, their signal intensities dropped remarkably. The presence of these entities is attributed to the hydrolysis process of $ZrCl_4$ precursor used in MOF synthesis, forming $ZrOCl_2$ trapped inside the MOF structure. Following the modification process, several washes were applied, resulting in $ZrOCl_2$ removal from the MOF structure. Regarding **Fig. S1c**, the C–N bond was fully detected (100%) in the pristine SURMOF (blank sample). However, post-synthetic treatment of the amino groups in the pristine SURMOF (blank sample) with stearic acid chloride resulted in their partial conversion into -NH-C18 groups, as displayed from the appearance of CNO bonds concurrently with CN bonds (red and blue peaks, **Fig. S2d**). Interestingly, **Fig. S2e** depicts the residual part of stearic acid chloride after reacting

with the amino groups in the pristine SURMOF, ensuring their successful conversion into the amide version.

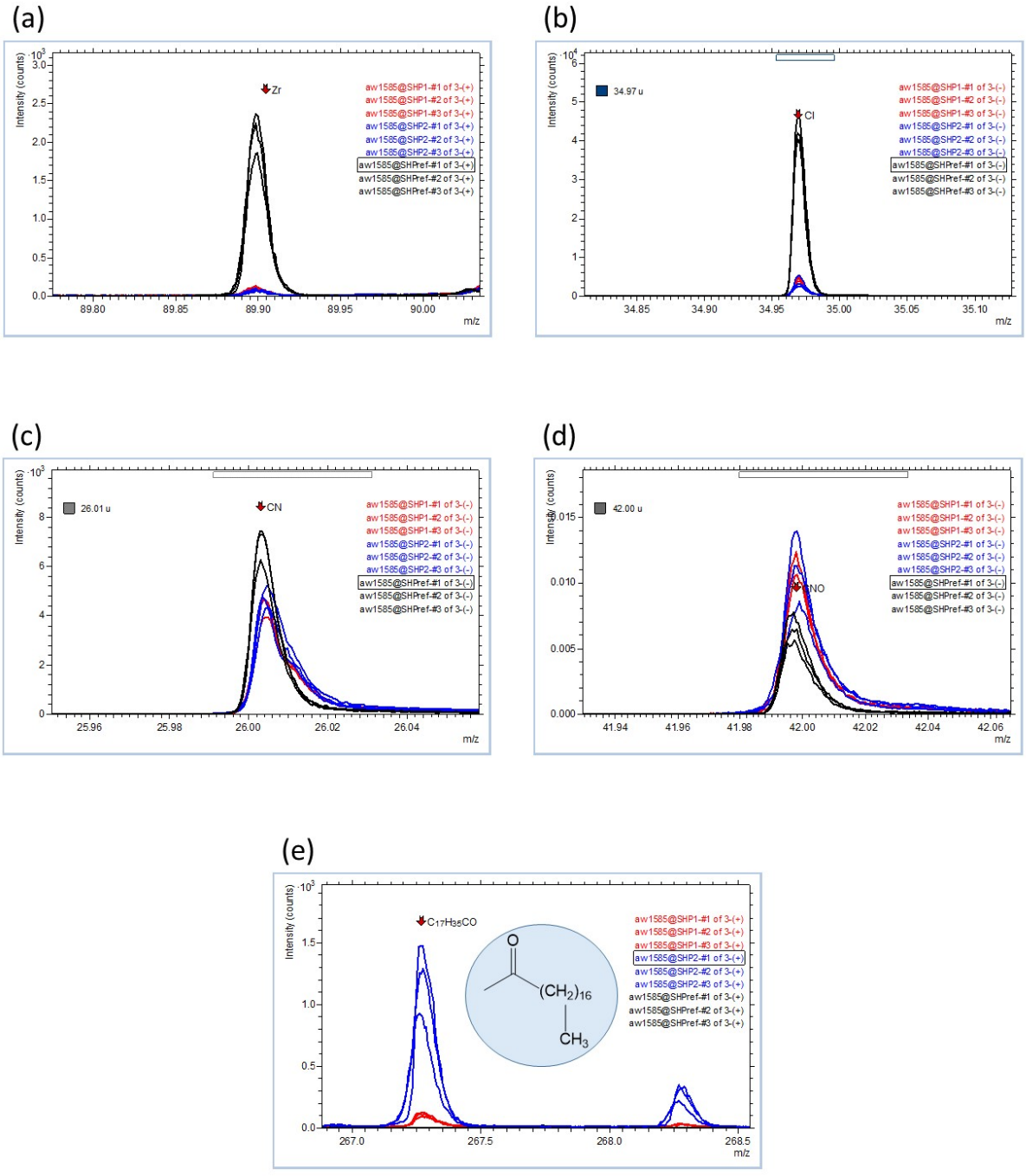

Fig. S2. ToF-SIMS results for pristine UiO-66-NH_2 SURMOF (blank sample in black) and its surface-modified counterpart (modified samples in blue and red), demonstrating (a-b) the high prevalence of Zr^{4+} and Cl^- in the blank sample before modification, which are washed away with (c) higher appearance of

amino groups in the blank sample, followed by (d) concurrent appearance of amino and amido groups in the modified samples in addition to (e) full proof of the amidation reaction by the existence of the residual part of stearic acid chloride.

XRD and IR results

XRD and IR were employed to study the surface modification of UiO-66-NH_2 SURMOF. **Fig. S3** displays modified C18@SURMOF referring to the pristine SURMOFs, along with the simulated XRD spectrum for the pristine SURMOF. Notably, the signal corresponding to the grafted -CH_2- is exemplified in IRRAS data.

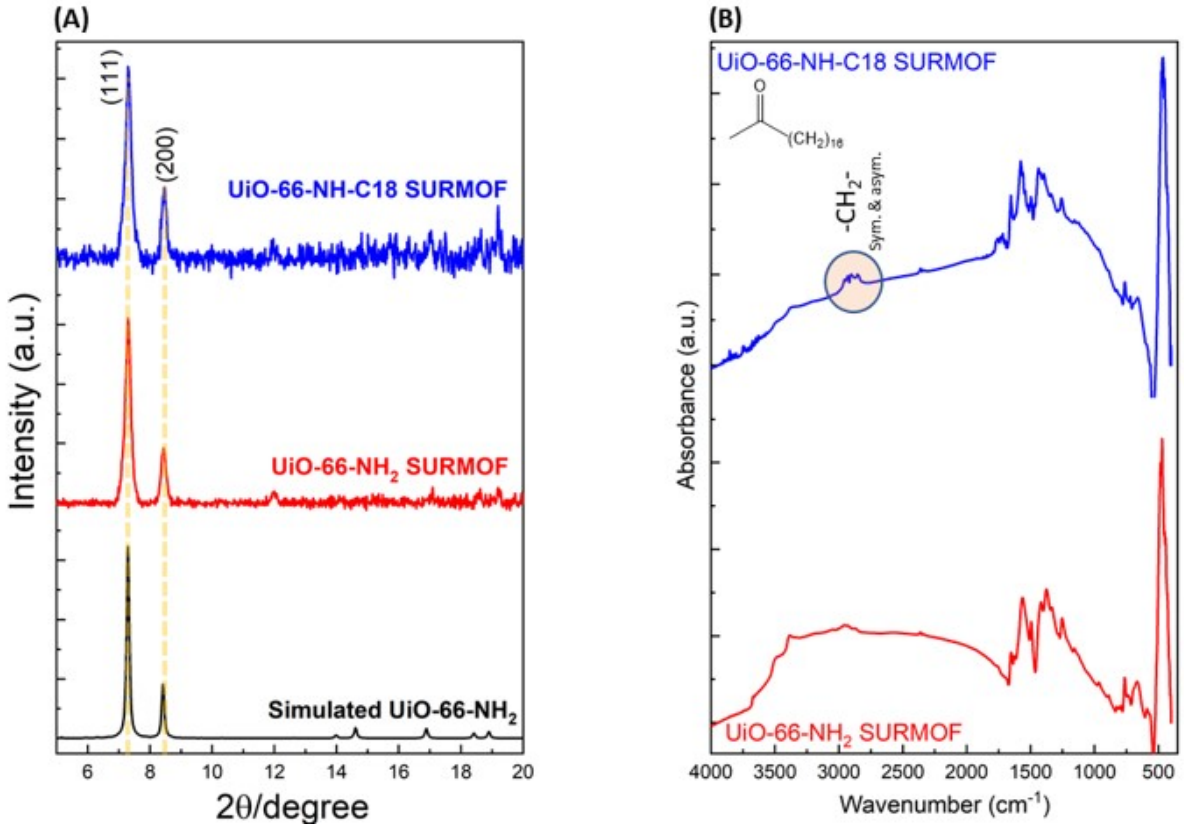

Fig. S3. (a) XRD patterns and (b) IRRAS data for the pristine SURMOF UiO-66-NH2 and the modified UiO-66-NH-C18.

Infrared Reflection-Absorption Spectroscopy (IRRAS)

The infrared reflection-absorption spectroscopy (IRRAS) technique was utilized to investigate the self-assembled monolayers (SAMs) of C18 (SAM@Au) and C18@SURMOF. The obtained IRRAS results revealed a notable shift in the CH stretching vibration of both samples, indicating differences in their molecular orientation on the surface. Specifically, for the long-chain alkanethiol, a well-ordered, pseudo-crystalline monolayer is expected to exhibit a peak position in the IRRA spectrum in the -CH region (2918.5 cm^{-1}) of the methylene asymmetric stretching, $\vartheta as(CH_2)$.[1] On the other hand, the shift of the peaks in the C18@SURMOF thin film (2913.3 cm^{-1} for $\vartheta as(CH_2)$) confirmed the disorder of the octadecanthiol (C18) chains.

As is well established, the surface selection rule governing IR spectroscopy of molecules in the vicinity of metal surfaces allows for the determination of the chemical composition of films and the alignment of individual molecules, including the tilting angle of alkane chains in relation to the substrate surface. [2] Consequently, the IRRAS technique provides robust evidence in support of the proposed entropy effect described in this study.

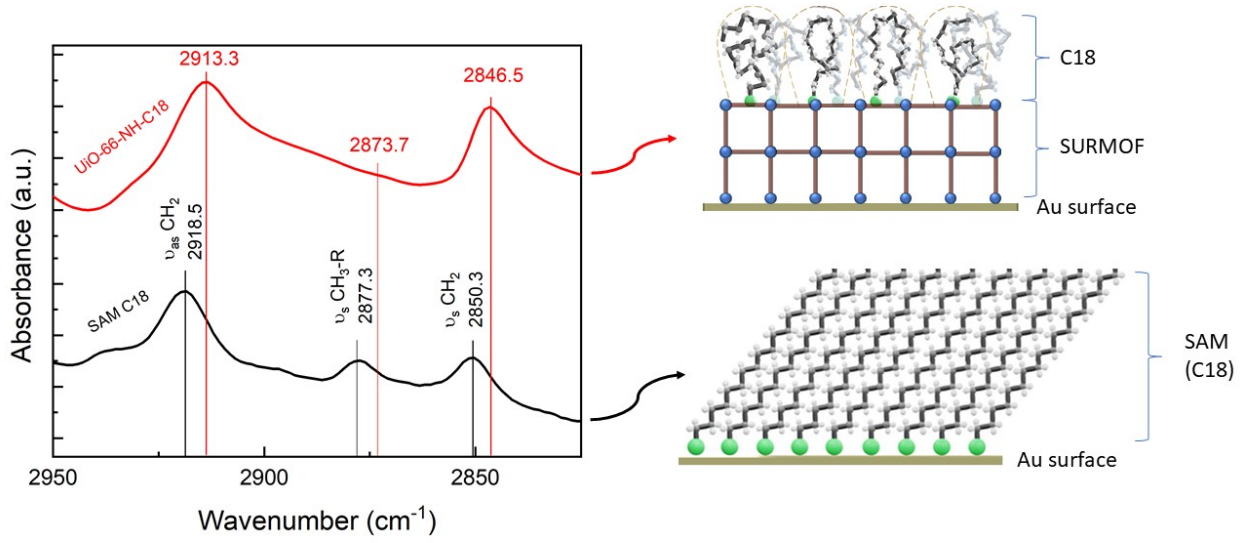

Fig. S4 The infrared reflection-absorption spectroscopy (IRRAS) results demonstrate the shift in the CH-region of self-assembled monolayers (SAM@Au) and C18@SURMOF. The spectrum shows a noticeable shift in the CH stretching vibration for both samples, confirm the disorder of the C18 on the surface of C18@SURMOF.

Surface Roughness Consistency before and after Post-Synthetic Modification

The atomic force microscope (AFM) analysis was conducted to assess the surface roughness of UiO-66-NH_2, C18F@SURMOF, and C18@SURMOF samples. The AFM results (Fig. S5) revealed no significant differences in the roughness values between the three samples. This finding suggests that the post-synthetic modification (PSM) did not induce notable alterations in the surface roughness of the SURMOF samples. The consistent roughness values across the samples indicate that the structural integrity and surface characteristics remained largely unchanged following the PSM process. These results underscore the robustness and stability of the synthesized SURMOF materials, which is essential for their potential applications in various fields.

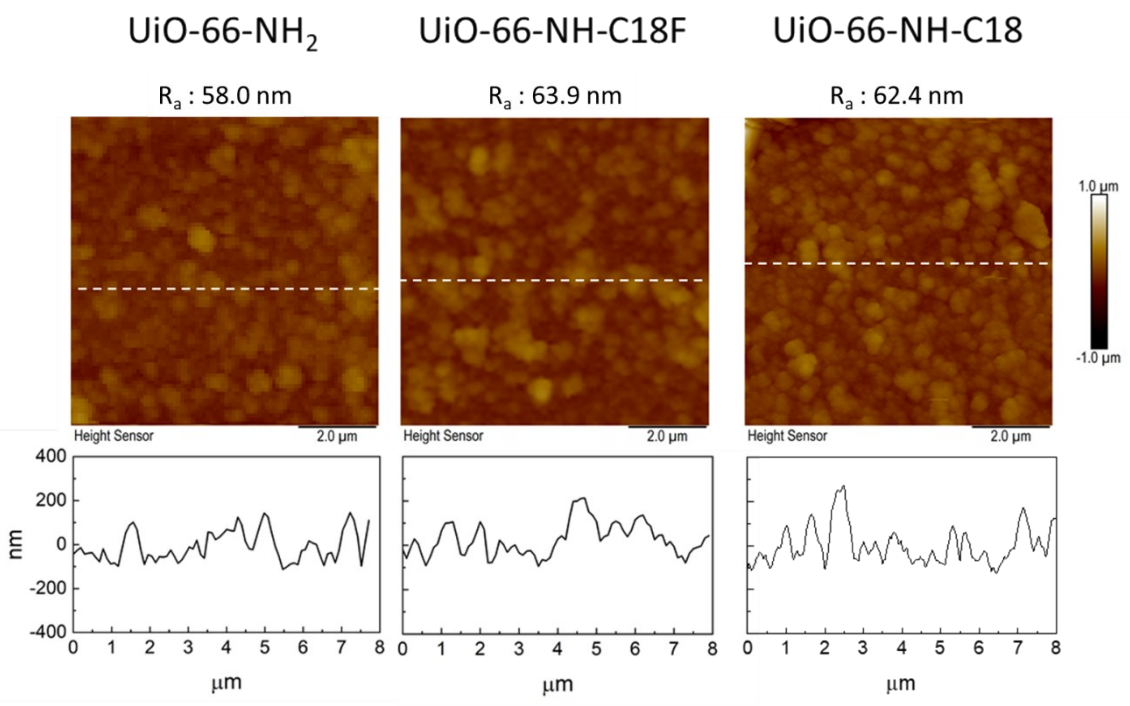

Fig. S5. AFM comparison of UiO-66-NH_2, C18F@SURMOF and C18@SURMOF.

Morphological Consistency before and after Post-Synthetic Modification

The scanning electron microscope (SEM) analysis was conducted to investigate the morphology of UiO-66-NH_2, C18F@SURMOF, and C18@SURMOF samples. Remarkably, the SEM images (Fig. S6) revealed striking similarities in the morphology of the three samples, with no noticeable differences discernible between them. This observation is consistent with the findings obtained from atomic force microscope (AFM) analysis. The comparable morphology across the three samples suggests a high degree of structural uniformity and stability, which are favorable characteristics for their potential applications in various fields. Moreover, this consistency in

morphology strongly indicates that the surface structure of the SURMOF remained unchanged following the post-synthetic modification (PSM).

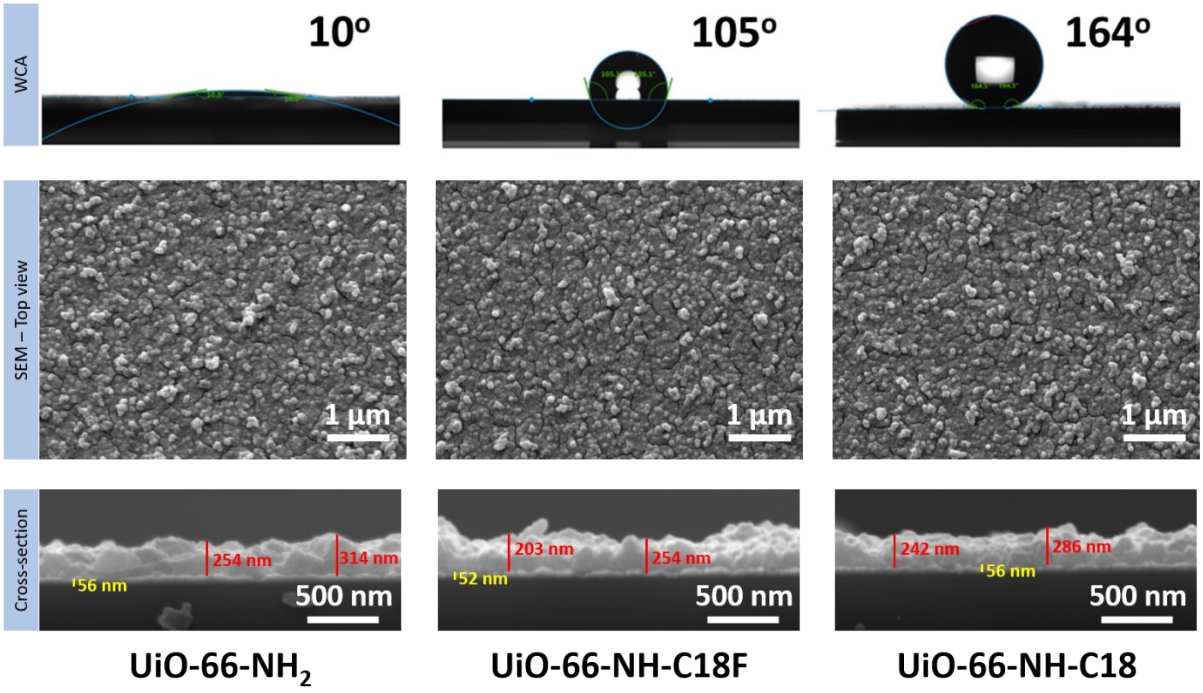

Fig. S6. SEM images and WCA of UiO-66-NH_2, C18F@SURMOF and C18@SURMOF.

Comparison of termination chemistry, topography, surface roughness, and water repelling performance of hydrophobic thin films from literature and this work

No.	Fabrication approach	Chemistry	Topography	Roughness (Ra/ Rq)		Contact Angle (°)	Ref.
				> 100 nm	< 100nm		
1.	Dip coating of PDMS@MOF@Cu mesh	Hydrocarbon	Micro/nano hierarchical	8.94 µm		151.8	[13]
2	Octadecylamine (ODA) modification in electodepositedMOF(Zn-BTC)- film	Hydrocarbon	Micro/nano hierarchical	~ 3 µm		153	[14]
3	Soot-templated fluorosilica protected with silicon microarmorprepared using photolithography	Fluorocarbon	Nano-structures within microstructure armor	Micro roughness		> 170	[15]
4	Zn-MOF film, subsequent fluoroalkylsilanecoating	Fluorocarbon	Micro/nano hierarchical	857 nm		155	[16]
5	Polymer multilayers coating	Hydrocarbon	Micro/nano hierarchical	~ 275 nm		138.0 ± 1.9	[17]
6	Polymer & SiO_2 nanoparticle crosslinked films	Hydrocarbon	Nano hierarchical	~ 175 nm		> 160	[18]
				~ 113 nm		~ 148	
7	Octyltrichlorosilane (OTS) self-assembled monolayer (SAM)	Hydrocarbon	i) micrometer-sized spikes of black silicon (bSi)	Micro roughness		> 160	[19]
			ii) Nanostructured SiO2 surface		0.21 nm	109	
8	Spin coating of silica particle with epoxy resin	Fluorocarbon	Nano hierarchical		96.5 nm	162 ± 3	[20]
9	Boehmite and aluminumacetylacetonatefilm with fluoroalkylsilanecoating	Fluorocarbon	Nano hierarchical		93 nm	152.5 ± 1.6	[21]
10	Solidification-induced phase separation ofpolysiloxane (PSO)/poly(dimethylsiloxane) (PDMS)	Hydrocarbon	Nanoporous		87.7 nm	155	[22]
11	Alkylsilane functionalized MOF (UIO-66-OH) films	Hydrocarbon	Nano hierarchical		73.9 nm	~ 112	[23]
12	Alkyl modified SURMOF (UIO-66-NH_2) films	Hydrocarbon	Nano hierarchical		31.4 nm	154.2	This work
					62.4 nm	155.3	
				~ 1 µm		164 ~ 166.7	

Table S1. WCA comparisons for hydrophobic thin films from literature and this work. WCA colored in red correspond to mediocre hydrophobicity and the rest corresponds to superhydrophobicity.[13-23]

Flexibility of hydrocarbon chains in dry conditions vs. during wetting

The flexibility of hydrocarbon chains corresponding to SAM@Au, C18F@SURMOF, and C18@SURMOF cases are reflected in the chain conformations. Due to the dense packing, the all-trans hydrocarbon chains in SAM@Au are stretched and tilted, whereas, in C18F@SURMOF and C18@SURMOF cases, the increased spacing among grafted anchor points allows for flexibility in the chains.

For the perfluorinated chains, the stronger repulsion of fluorine atoms in -CF_2- groups over the hydrogen in -CH_2- groups practically stretches the hydrocarbon chains. The enhanced rigidity for CF chains attributes to a greater thickness of 0.4 nm of CH film.

When SAM@Au comes into contact with a water droplet, the hydrocarbons form a dense insulating layer, whereas the pristine SURMOF adsorbs water. In the cases of C18F@SURMOF and C18@SURMOF, the perfluorinated hydrocarbon chains are mixed with water "pins" which plug into the polymer brush, while in C18@SURMOF, the clear separation of water and hydrocarbon chains facilitate a much higher water contact angle.

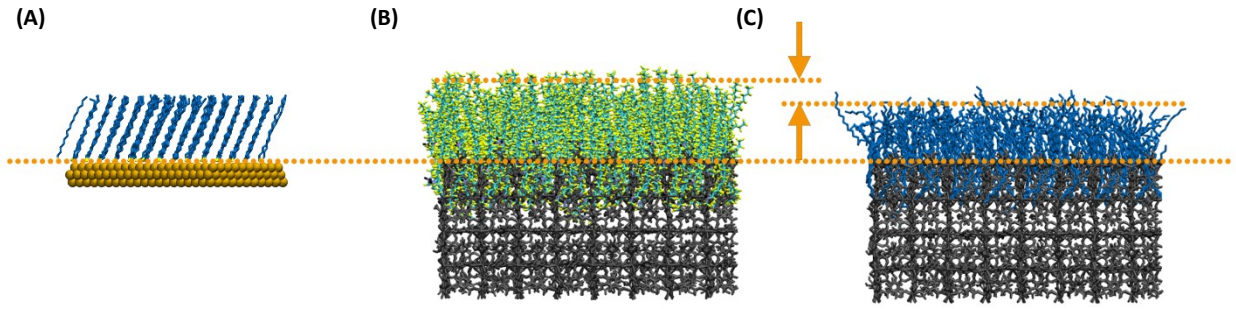

Fig. S7. The stretching of hydrocarbon chains in the dry conditions for (A) SAM@Au, (B) C18F@SURMOF, and (C) C18@SURMOF. The substrates are aligned, marked by the orange dotted line across the three systems, whereas the distinguished thicknesses between C18F@SURMOF and C18@SURMOF are illustrated by orange arrows. This difference in chain stretching is measured at 0.4 nm due to the stronger repulsion among fluorine atoms in CF chains, exemplifying a lower entropy in CF

chains. The fluorine atoms are explicitly shown in bright yellow, whereas hydrogen atoms on hydrocarbon chains are omitted for clarity.

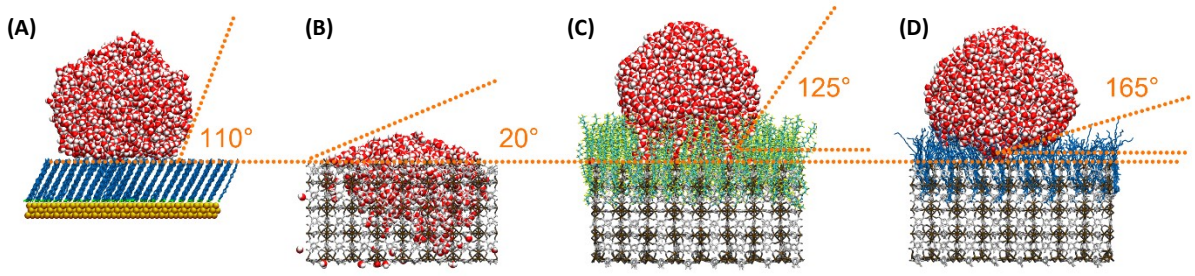

Fig. S8. Water contact angles in the wetting simulations for (A) SAM@Au, (B) SURMOF, (C) C18F@SURMOF, and (D) C18@SURMOF. The substrates are aligned, marked by the orange dotted line across the four systems. The water contact angles are marked by orange dotted lines. Particularly, in the case of C18F@SURMOF and C18@SURMOF, the water droplet cannot react to the reference surface on the substrate, where additional baselines are indicated by horizontal orange dotted lines. For better clarity, MOF linkers are shown in light gray.

Intrinsic entropy of hydrocarbon chains from Ramachandran plots

The intrinsic entropy corresponding to SAM@Au, C18F@SURMOF, and C18@SURMOF cases are calculated from the conformational phase space. The torsional angles on the C-C back-bone of hydrocarbons statistically fall in the categories of trans-trans (180 deg – 180 deg), trans-gauche (60 deg – 180 deg) and gauche-gauche (60 deg – 60 deg) conformations. In dry conditions, SAM is mostly in an all-trans conformation, denoted by the highly concentrated distribution at the 180 deg – 180 deg extremities of the quadrants in the Ramachandran plot, whereas the occurrences of gauche defects are very rare. In contrast, for C18F@SURMOF and C18@SURMOF cases, the conformers cover increasingly larger phase space areas with a diminishing trans-trans density.

The entropy is then estimated based on the occurrence probability for individual states across the phase space as entropy $S = -k_b \Sigma_i p_i ln p_i$ where p_i is the estimated kernel density over all

conformers. Consistently, the estimated entropy ranks SAM@Au, C18F@SURMOF, and C18@SURMOF with an increasing disorder of 5.3^{k_b}, 6.47^{k_b}, and 6.97^{k_b}. The number of gauche defects per chain is calculated based on the occurrence probability as an average of 0.04 gauche defects per hydrocarbon chain in SAM@Au, 1.42 per chain for C18F@SURMOF, and 2.89 per chain for C18@SURMOF.

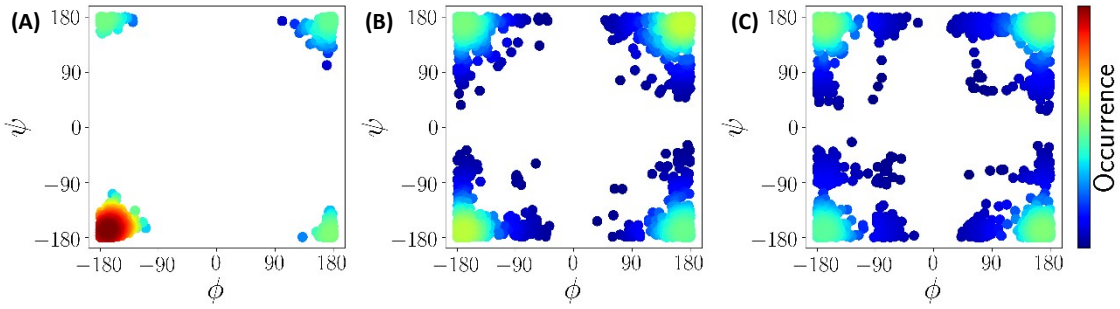

Fig. S9. Ramachandran plots for the torsional angles of the C-C backbone in the dry conditions for (A) SAM@Au, (B) C18F@SURMOF, and (C) C18@SURMOF. Color-coded is the occurrence frequencies of individual states. The SAM is in all-trans states where the torsional angles are constrained to the π-π corners in all quadrants, whereas for C18F@SURMOF and C18@SURMOF, there exist numerous gauche defects. The entropy calculated based on the state occurrence frequencies ranks the SAM as the least entropic at 5.3^{k_b}, the C18F@SURMOF in the middle with an entropy reference at 6.47^{k_b}, and C18@SURMOF with the highest entropy at 6.97^{k_b}. In dry conditions, the number of gauche defects per chain is 0.04 for SAM, 1.42 for C18F@SURMOF, and 2.89 for C18@SURMOF.

Determination of surface density of C18 and C18F chains in UiO-66-C18(F) SURMOFs

To determine the grafted density in C18F@SURMOFs, the intensity of the CH_2 stretching vibration at 2929 cm^{-1} originating from to the MUD-SAM used to functionalize the Au substrate prior to SURMOF deposition was compared to the intensity of the C-F stretching vibration at 1151 cm^{-1} corresponds to the grafted hydrocarbons, see Fig. S10. Using results from theory on the IR vibrational modes (see Fig. S11) the ratio of monomer coverage in MUD-SAM vs C18F ratio is determined as 0.7:1, i.e. the surface density of C18F is comparable to the density in the MUD-

SAM. Note, that this is only a semiquantitative estimate since other effects (e.g. scattering of IR light passing through the SURMOF) may lead to errors. Nevertheless, our calculated surface density of C18F is also consistent with the density of partially fluorinated SAM reported in ref.[24]

For the determination of the surface density in the C18@SURMOF, the situation is more difficult as the CH_2 signals in the MUD-SAM and the C18 chains overlap. Moreover, the surface selection rules[25] makes estimation of CH chain densities more complex as the C18s are coiled. Considering both factors, we conclude the surface density of grafted C18F and C18 are consistent with the setup in the MD simulations.

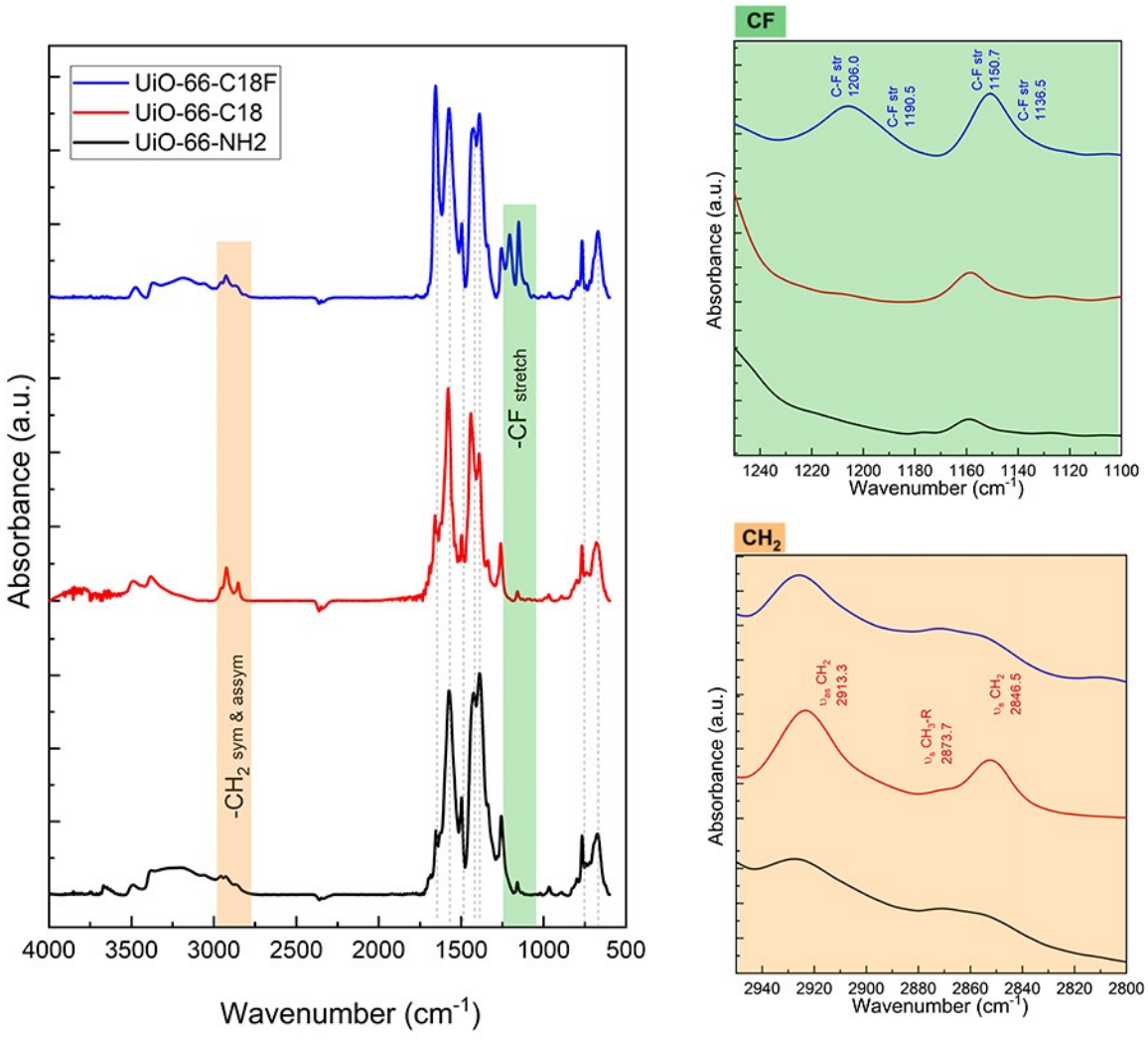

Fig. S10. IRRAS data recorded for f UiO-66-NH_2, C18@SURMOF and C18F@SURMOF.

For reference, isolated C18 and C18F chains in the linear (trans) conformation are structurally optimized with density functional theory (DFT) before the vibrational intensities corresponding to their unique peaks in the IR spectrum were calculated. The geometry optimization were performed with PBE0 hybrid functional under tight convergence criterion (tightSCF) in Orca version 5.0.4.

The optimized CH chain correspond to the all-trans configuration and the optimized CF chain corresponds to the helical configuration in Fig. S11.

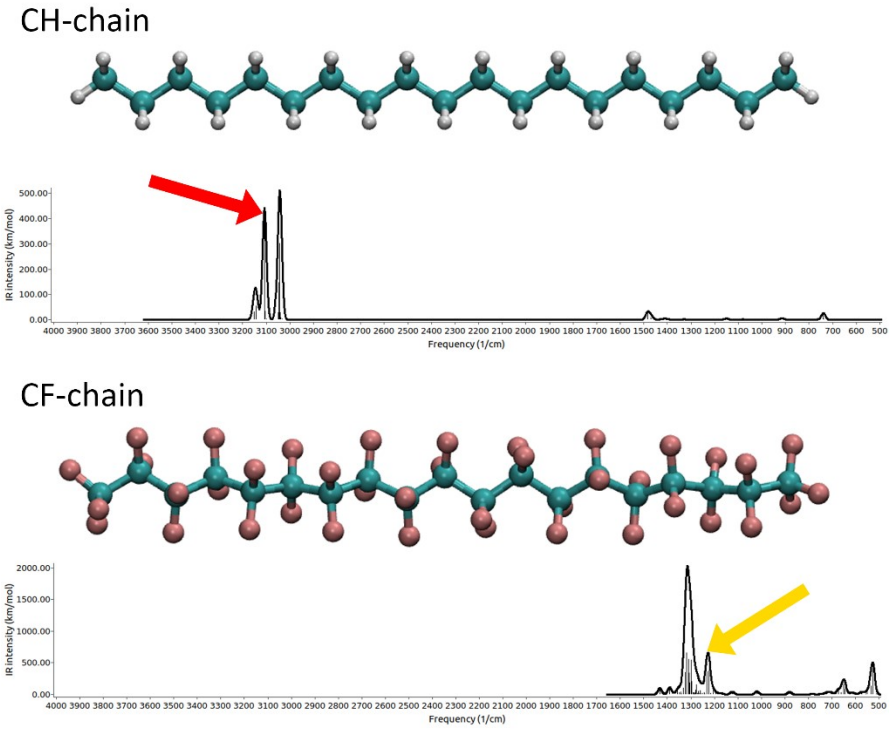

Fig. S11. DFT optimized molecular geometries and corresponding IR spectra for isolated chains.

After reaching global minimum, the vibrational modes were obtained using numerical Hessian calculations. To compare with experimental IRRAS spectra, discrete IR peaks from DFT are integrated with Gaussian broadening with band width of 20 cm^{-1}. The unique peaks for CH: at 3144 cm^{-1}, marked by the red arrow; and CF: at 1227 cm^{-1}, marked by the yellow arrow, are selected in the calculation the CH and CF surface densities.

Furthermore, we have performed X-ray photoelectron spectroscopy measurements on our pristine UiO-66-NH2 SURMOF, C18 grafted SURMOF and C18F grafted SURMOFs, in Fig. S12. With

C1s spectra (Fig. S12B), we were able to fit the XPS peaks by individual C-H and C-F signals and determine a 1:1.43 ratio between the grafted C18 and C18F chains, consistent with the IRRAS-based estimation of surface density. As the SURMOF is insulating, considerable charge effect renders energy shifts among samples, in particular for the O1s, N1s, and Zr3d spectra in Fig. S12E-G.

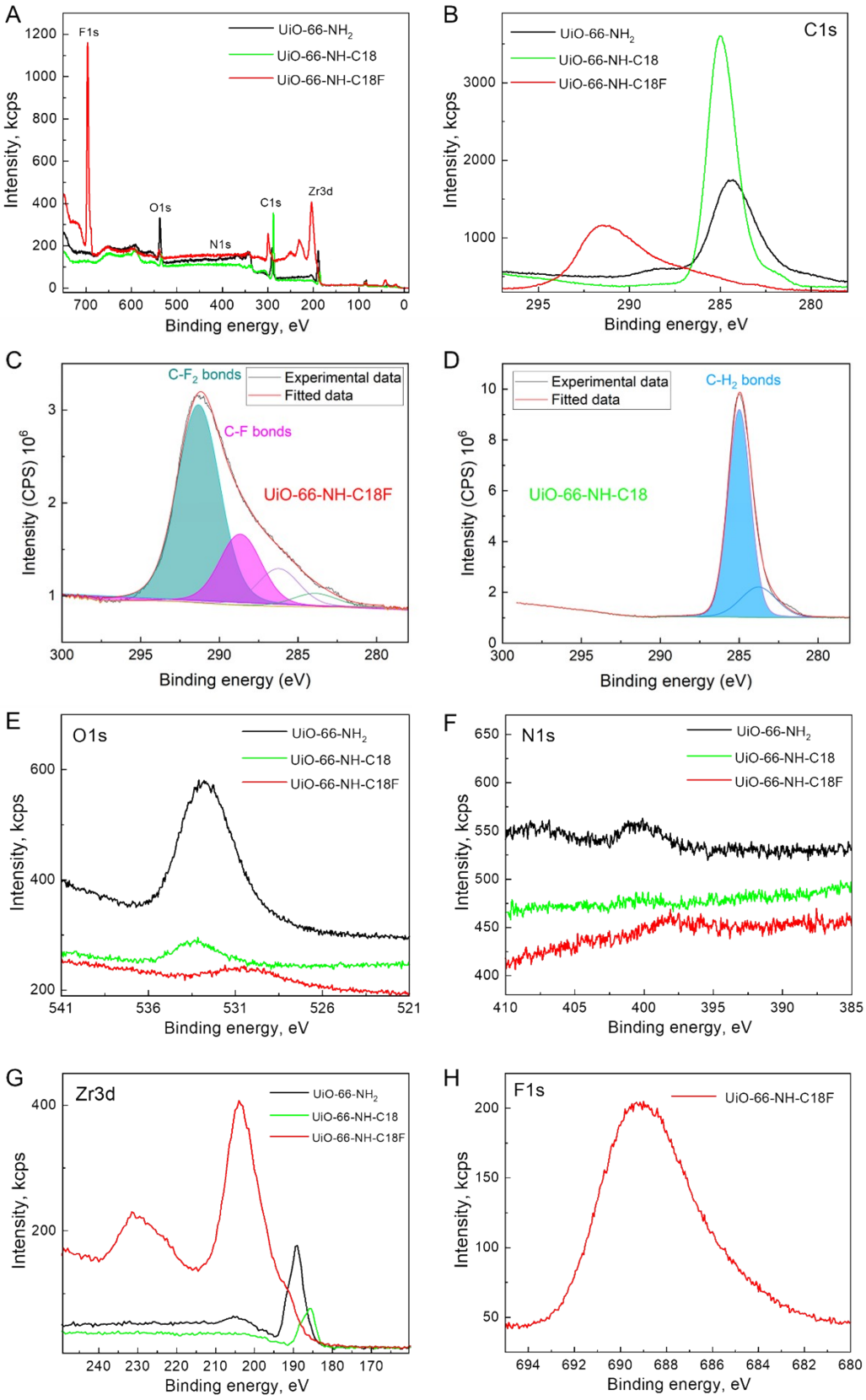
A
F1s
O1s
N1s
C1s
Zr3d
UiO-66-NH2
UiO-66-NH-C18
UiO-66-NH-C18F
Intensity, kcps
Binding energy, eV
B
C1s
C
C-F2 bonds
C-F bonds
Experimental data
Fitted data
UiO-66-NH-C18F
Intensity (CPS) 10^6
Binding energy (eV)
D
C-H2 bonds
UiO-66-NH-C18
E
O1s
F
N1s
G
Zr3d
H
F1s

Figure S12. (A) Wide-scan XPS spectrum of the prepared SURMOFs with an excitation energy of 850 eV. (B) C1s XPS spectra recorded for the prepared SURMOFs with an excitation energy of 450 eV. (C-D) C1s XPS spectra recorded with an excitation energy of 450 eV for C) UiO-66-NH-C18F D) UiO-66-NH-C18. (E) O1s XPS spectra at 533 eV recorded for the prepared SURMOFs with an excitation energy of 650 eV. (F) N1s XPS spectra at 399.5 eV recorded for the prepared SURMOFs with an excitation energy of 550 eV. (G) Zr3d XPS spectra at approx. 190 eV recorded for the prepared SURMOFs with an excitation energy of 330 eV. (H) F1s XPS spectra at 689 eV recorded for the prepared C18F@UiO-66-NH2 with an excitation energy of 850 eV.

Movies of the molecular dynamics simulation for wetting

For the pristine SURMOF, water is adsorbed in the MOF. The SURMOF is grafted on both sides to show the dynamics of flexible hydrocarbons in dry and wetted conditions.

Movie S1. Dynamic wetting of the water in MD simulations for water droplet on (A) pristine SURMOF, (B) C18F@SURMOF, and (C) C18@SURMOFs.

Movie of a water droplet rolling off the superhydrophobic C18@SURMOF

A water droplet is placed on the superhydrophobic C18@SURMOF sample and upon tiling the substrate, the droplet quickly rolls off. The slow-motion movie corresponds to 0.1x real time playback speed.

Movie S2. Rolling of water droplet (volume 5 μL) on superhydrophobic C18@SURMOF.

References

1. Hashem, T., et al., *Liquid‐Phase Quasi‐Epitaxial Growth of Highly Stable, Monolithic UiO‐66‐NH2 MOF thin Films on Solid Substrates.* ChemistryOpen, 2020. **9**(5): p. 515.
2. Bhadra, P. and S.W.I. Siu, *Comparison of Biomolecular Force Fields for Alkanethiol Self-Assembled Monolayer Simulations.* The Journal of Physical Chemistry C, 2017. **121**(47): p. 26340-26349.
3. Boyd, P.G., et al., *Force-field prediction of materials properties in metal-organic frameworks.* The journal of physical chemistry letters, 2017. **8**(2): p. 357-363.
4. Li, Z., et al., *Ionic Liquid/Metal–Organic Framework Composites for H2S Removal from Natural Gas: A Computational Exploration.* The Journal of Physical Chemistry C, 2015. **119**(7): p. 3674-3683.
5. Vazquez, M., et al., *Structural and Dynamic Insights into the Conduction of Lithium-Ionic-Liquid Mixtures in Nanoporous Metal–Organic Frameworks as Solid-State Electrolytes.* ACS Applied Materials & Interfaces, 2021. **13**(18): p. 21166-21174.
6. Dodda, L.S., et al., *LigParGen web server: an automatic OPLS-AA parameter generator for organic ligands.* Nucleic acids research, 2017. **45**(W1): p. W331-W336.
7. Iannuzzi, M., A. Laio, and M. Parrinello, *Efficient Exploration of Reactive Potential Energy Surfaces Using Car-Parrinello Molecular Dynamics.* Physical Review Letters, 2003. **90**(23): p. 238302.
8. Prieve, D.C. and W.B. Russel, *Simplified predictions of Hamaker constants from Lifshitz theory.* Journal of Colloid and Interface Science, 1988. **125**(1): p. 1-13.
9. Hoover, W.G., *Canonical dynamics: Equilibrium phase-space distributions.* Physical review A, 1985. **31**(3): p. 1695.
10. Andersen, H., *Molecular dynamics at constant temperature and/or pressure.* J. Chem. Phys, 1980. **72**: p. 2384.
11. Stewart, J.J., *Optimization of parameters for semiempirical methods VI: more modifications to the NDDO approximations and re-optimization of parameters.* Journal of molecular modeling, 2013. **19**(1): p. 1-32.
12. Li, H., et al., *Dynamic contact angles and mechanisms of motion of water droplets moving on nanopillared superhydrophobic surfaces: a molecular dynamics simulation study.* Langmuir, 2018. **34**(34): p. 9917-9926.
13. Wang, M., et al., *Construction of super-hydrophobic PDMS@MOF@Cu mesh for reduced drag, anti-fouling and self-cleaning towards marine vehicle applications.* Chemical Engineering Journal, 2021. **417**.
14. Zhao, Y. and J.-M. Hu, *Double Immobilized Superhydrophobic and Lubricated Slippery Surface with Antibacterial and Antifouling Properties.* ACS Applied Bio Materials, 2023. **6**(8): p. 3341-3350.
15. Wang, D., et al., *Design of robust superhydrophobic surfaces.* Nature, 2020. **582**(7810): p. 55-+.
16. Telmenbayar, L., et al., *Development of mechanically robust and anticorrosion slippery PEO coating with metal-organic framework (MOF) of magnesium alloy.* Chemical Engineering Journal, 2023. **458**.
17. Bechler, S.L. and D.M. Lynn, *Reactive Polymer Multi layers Fabricated by Covalent Layer-by-Layer Assembly: 1,4-Conjugate Addition-Based Approaches to the Design of Functional Biointerfaces.* Biomacromolecules, 2012. **13**(5): p. 1523-1532.
18. Li, X., et al., *Nonfluorinated, transparent, and spontaneous self-healing superhydrophobic coatings enabled by supramolecular polymers.* Chemical Engineering Journal, 2021. **404**.

19. Lepikko, S., et al., *Droplet slipperiness despite surface heterogeneity at molecular scale.* Nature Chemistry, 2024. **16**(4).
20. Zhao, X., et al., *Robust, transparent, superhydrophobic coatings using novel hydrophobic/hydrophilic dual-sized silica particles.* Journal of Colloid and Interface Science, 2020. **574**: p. 347-354.
21. Nakajima, A., et al., *Preparation of transparent superhydrophobic boehmite and silica films by sublimation of aluminum acetylacetonate.* Advanced Materials, 1999. **11**(16): p. 1365-1368.
22. Wang, D., et al., *Highly Transparent and Durable Superhydrophobic Hybrid Nanoporous Coatings Fabricated from Polysiloxane.* Acs Applied Materials & Interfaces, 2014. **6**(13): p. 10014-10021.
23. Singh, V., X.H. Men, and M.K. Tiwari, *Transparent and Robust Amphiphobic Surfaces Exploiting Nanohierarchical Surface-grown Metal-Organic Frameworks.* Nano Letters, 2021. **21**(8): p. 3480-3486.
24. Lu, H., et al., *Structure of Self-Assembled Monolayers of Partially Fluorinated Alkanethiols with a Fluorocarbon Part of Variable Length on Gold Substrate.* The Journal of Physical Chemistry C, 2013. **117**(37): p. 18967-18979.
25. Arnold, R., A. Terfort, and C. Wöll, *Determination of Molecular Orientation in Self-Assembled Monolayers Using IR Absorption Intensities: The Importance of Grinding Effects.* Langmuir, 2001. **17**(16): p. 4980-4989.